Journal of
Materials Chemistry C

Accepted Manuscript

Volume 4 | Number 1 | 7 January 2016 | Pages 1–224

Journal of
Materials Chemistry C

Materials for optical, magnetic and electronic devices
www.rsc.org/MaterialsC

ISSN 2050-7526

ROYAL SOCIETY OF CHEMISTRY

PAPER
Nguyễn T. K. Thanh, Xiaodi Su et al.
Fine-tuning of gold nanorod dimensions and plasmonic properties using the Hofmeister effects

175 YEARS

This is an Accepted Manuscript, which has been through the Royal Society of Chemistry peer review process and has been accepted for publication.

Accepted Manuscripts are published online shortly after acceptance, before technical editing, formatting and proof reading. Using this free service, authors can make their results available to the community, in citable form, before we publish the edited article. We will replace this Accepted Manuscript with the edited and formatted Advance Article as soon as it is available.

You can find more information about Accepted Manuscripts in the author guidelines.

Please note that technical editing may introduce minor changes to the text and/or graphics, which may alter content. The journal's standard Terms & Conditions and the ethical guidelines, outlined in our author and reviewer resource centre, still apply. In no event shall the Royal Society of Chemistry be held responsible for any errors or omissions in this Accepted Manuscript or any consequences arising from the use of any information it contains.

ROYAL SOCIETY OF CHEMISTRY

rsc.li/materials-c

Journal Name

ARTICLE

Intramolecular Non-Covalent Interactions as a Strategy Towards Controlled Photoluminescence in Copper(I) Complexes†

G. A. Filonenko,[a] R. R. Fayzullin[b] and J. R. Khusnutdinova[a,*]

In this work we describe a new strategy for designing photoluminescent Cu(I) complexes. At its core are simple cyclophane inspired N-donor ligands featuring intramolecular interactions between aromatic units within a single molecule. Variation of the steric bulk inflicted a change of intramolecular stacking distances, that in turn affected the emission colour of copper(I) complexes tunable in a 0.5 eV range from green to red. As the interactions driving emission are confined to the single molecule, no intermolecular aggregation is required to enable photoluminescence in solution, pristine crystals, or solution-cast polymer films. Crystallographic study provides a link between the spatial proximity of the aromatic rings of the ligands (ranging from 3.349 to 3.731 Å) and the enhancement of emission efficiency, which increases dramatically from 0.02 to 0.78 at 296 K as the rings spacing contracts. Photophysical and theoretical analyses confirm the involvement of intramolecular interactions in the formation of the emissive state and describe the observed phenomena on a molecular level.

Introduction

The vast class of photoluminescent (PL) compounds holds great importance in modern technology. Comprised of purely organic molecules or transition metal complexes, luminescent compounds have found broad application in light emitting devices,[1] smart materials for sensing[2] and imaging applications.[3, 4] As the demand for such emitters steadily grows, new strategies for designing PL materials and modulating their properties become increasingly important.

Conventional transition metal (TM)-based luminophores rely heavily on the use of π-extended ligands required to create the desired bandgap that facilitates excitation and emission. This design strategy yielded remarkably efficient PL complexes with recent examples including Ir,[5] Pt,[6, 7] Zn,[8] and Au[9]. Since noble metals currently comprise the most numerous class of TM-based PL complexes, the search for a cheap yet efficient and sustainable alternative remains an important objective.[10]

Over the last two decades, Cu(I) complexes have been recognized as a sustainable alternative to noble metal-based PL materials.[11-14] These compounds include mono- and binuclear complexes with chelating phosphines,[15-18] mononuclear phenanthroline-[19-21] or diimine-based complexes[22] and trigonal NHC-based and amide-bound ligands.[23-29] Similar to the rest of the TM-based emitters, the control over emissive properties in Cu(I) compounds is typically achieved by tuning the electronic properties of their ligands[30, 31] or addressing the ligand conformational dynamics.[32] This implies that the emission of TM-complexes mainly relies on covalent interactions within one molecule while the intermolecular and non-covalent interactions typically remain unutilized.
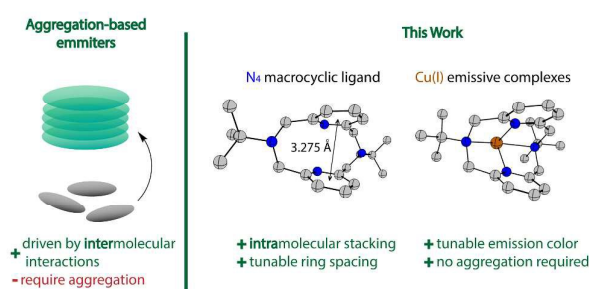
Figure 1. Comparison between *inter-* and *intramolecular* interactions as the driving factor for photoluminescence. Structure of **L1** pyridinophane macrocycle (N₄) adopted from Ref. 33.

One conceptually opposite approach for designing PL compounds makes use of the *intermolecular* non-covalent interactions. Coined in 2001 by Tang, this strategy is referred to as Aggregation Induced Emission (AIE) and it exploits the

[a.] Coordination Chemistry and Catalysis Unit, Okinawa Institute of Science and Technology Graduate University, 1919-1 Tancha, Onna-son, Kunigami-gun, Okinawa, 904-0495 Japan
[b.] A.E. Arbuzov Institute of Organic and Physical Chemistry, Kazan Scientific Center, Russian Academy of Sciences, Arbuzov Street, 8, Kazan 420088, Russian Federation
* corresponding author

ARTICLE

intermolecular arrangement in solid or aggregated state to enable photoluminescence.[34, 35] This arrangement can, for example, restrict the molecular motions responsible for non-radiative relaxation or induce photoluminescence in π-π stacked assemblies that emit when aggregated in contrast to the non-emissive isolated molecular state.

The AIE behaviour is not limited to organic dyes and can be found in TM complexes. For example, non-covalent interactions were found to contribute to emission of Zn, Au, Pt, Ir, Al and Cu compounds.[36-41] However, with very few exceptions,[42, 43] the non-covalent interactions involved in modulating photoluminescence are *intermolecular* and therefore are highly sensitive to the structure of the bulk material and thus hard to control and rarely translated to solution state.

Potentially one can overcome the limitations of the AIE approach if the non-covalent interactions driving the emission are *intramolecular* and therefore not affected by intermolecular arrangement. Such intramolecular interactions can be found in pyridinophane macrocycles (e.g. N,N'-dialkyl-2,11-diaza[3.3](2,6)-pyridinophane, Figure 1). For example, the N-*tert*-butyl substituted pyridinophane ligand is conformationally flexible in transition metal complexes[44, 45] and features tight π-π spacing of 3.275 Å between two pyridine rings in the solid state in the free ligand (Figure 1). If the interaction between non-conjugated pyridine rings can be utilized to enable emission in TM-complexes, the use of pyridinophane ligands would mark a conceptually new strategy for designing emissive TM complexes based on purely non-covalent interactions.

In this work, we demonstrate that such intramolecular interactions can be successfully employed to design a new class of photoluminescent Cu(I) complexes. The colour and quantum yield of the emission could be altered by controlling the conformation of the pyridinophane macrocyclic ligand by simply varying N-substituents (R group, Figure 1). Namely, the variation of the spatial proximity of two non-conjugated pyridine rings within the macrocycle allowed for emission in a wide range of 524-665 nm with the quantum yield reaching 0.74 at room temperature. The photoluminescence of the complexes most emissive in the solid state was also successfully translated to dichloromethane solutions, thus overturning the prerequisite for emitters driven by the non-covalent interactions to be in the aggregated state.

Experimental Section

All manipulations unless stated otherwise were performed using Schlenk or glovebox techniques under dry argon atmosphere. Anhydrous solvents were dispensed from an MBRAUN solvent purification system and degassed prior to use. Anhydrous deuterated solvents were purchased from Eurisotop and stored over 4Å molecular sieves. All chemicals unless noted otherwise were purchased from major commercial suppliers (TCI, Sigma-Aldrich and Nacalai Tesque) and used without purification. Ligand **L1**,[33] 2,11-diaza[3.3](2,6)pyridinophane (**L$_{NH}$**)[46] and NaBArF (sodium

tetrakis[3,5-bis(trifluoromethyl) phenyl]borate)[47] were prepared according to literature procedures. [Cu(MeCN)$_4$]$^+$ precursors were prepared by dissolving Cu$_2$O in acetonitrile solutions in the presence of aqueous HBF$_4$ or HPF$_6$ followed by two consecutive recrystallizations from cold acetonitrile.[48]

Polymer blends of complexes **4-6** were prepared by mixing saturated solution of 2-3 mg of the corresponding complex in CH$_2$Cl$_2$ with 1 mL of PMMA (poly(methyl methacrylate)) solution in CH$_2$Cl$_2$ containing ca. 100 mg of the polymer. The films were prepared from these blends by drop casting in a rectangular PTFE mold followed by drying in vacuo.

Instrumentation: NMR spectra were measured on JEOL ECZ600R 600MHz, JEOL ECZ400S 400 MHz and Bruker Avance II 400 MHz spectrometers. Full spectra are available from the Supporting Information. Electrospray Ionization Mass Spectrometry (ESI-MS) measurements were performed on a Thermo Scientific ETD apparatus. Elemental analyses were performed using an Exeter Analytical CE440 instrument.

The photoluminescence measurements in degassed dichloromethane solutions at varying concentrations were performed using a Hitachi F7000 apparatus. Absorbance spectra were collected using an Agilent Cary 60 machine. Photoluminescence lifetime measurements were performed using the second harmonics of Spectra-Physics Mai Tai pulsed laser and a Hamamatsu Photonics Streak Scope camera. The decay data were fitted with a single exponential decay function unless specified otherwise. The same laser light source equipped with a Thorlabs IS236A integrating sphere and an OceanOptics USB4000-ES spectrometer was used for quantum yield measurements in solutions (CH$_2$Cl$_2$, c = 0.5-1 μM) and in the solid state. The accuracy of quantum yield data was confirmed using a Hamamatsu Photonics Quantaurus-QY system that established the variations in absolute QY to be within 5% for solid and solution samples. Emission spectra were recorded using OceanOptics USB4000-ES (solutions, Figure 6B) or Hamamatsu Photonics Streak Scope camera (solids, Figure 6A). The IR spectra were recorded using Cary 630, ATR module. Cyclic voltammetry (CV) studies were performed with an ALS/CHI Electrochemical Analyzer 660E. Electrochemical grade NBu$_4$ClO$_4$ supplied by Sigma-Aldrich was used as the supporting electrolyte. Electrochemical measurements were performed under nitrogen after the sample solutions were purged with nitrogen for 10 minutes. A glassy carbon disk electrode (GCE; *d* = 1.6 mm) was used as the working electrode, and a Pt wire as the auxiliary electrode. The non-aqueous Ag-wire reference electrode assembly was filled with 0.01 M AgNO$_3$/0.1 M NBu$_4$ClO$_4$/MeCN solution. The reference electrodes were calibrated against ferrocene. The ferrocene peak separation in acetonitrile and in CH$_2$Cl$_2$ solution was 105 and 210 mV at 23 °C, respectively.

Methods used for DTF calculations and optimized geometries can be found in section S4 of the Supporting Information.

X-ray diffraction data for single crystal samples was collected on a Rigaku XtaLab PRO instrument using graphite monochromated MoKα radiation (0.71073 Å) at -180 °C. Fragments of the main residues of complexes **2**, **3** and **6** and anionic fragments in **3** and **6** were disordered and reported in

Journal Name

ARTICLE

full in the Supporting information. Complex **2** crystallizes as an acetonitrile solvate. Complex **3** contained two independent molecules in the asymmetric cell. Section S5 of the Supporting Information contains full experimental details regarding data collection and structure refinement.

Results and Discussion

Synthesis and structure.

Pyridinophane macrocycles can be prepared with various alkyl or functionalized substituents using modifications of known synthetic protocols.[33, 46] We produced a set of ligands bearing bulky *tert*-butyl substituents (**L1**) and less bulky ester (**L2**) and alcohol functionalized (**L3**) side chains. In acetonitrile solutions **L1**-**L3** rapidly react with [Cu(MeCN)$_4$]$^+$ precursors to form bright orange solutions of cationic acetonitrile complexes **1**-**3** (Scheme 1).

**Scheme 1**. Synthesis of cationic Cu complexes **1**-**3**
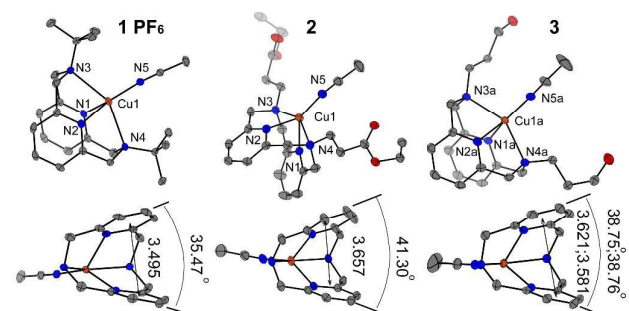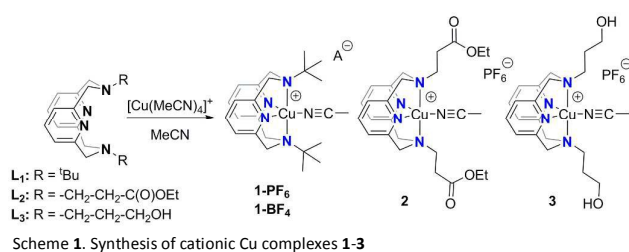
Figure 2. Solid state structures of cationic Cu complexes **1**-**3**. Thermal ellipsoids are shown on 50% probability level, hydrogen atoms, minor disordered fragments, solvent molecules and anions are omitted for clarity. Ring-ring spacing given for centroids, substituents at amine groups are omitted in the side view projections. For complex **3** containing two molecules per the asymmetric cell only one molecule is shown. Selected bond lengths and angles (Å, °): **1PF$_6$**: Cu1-N1 2.089(2), Cu1-N2 2.099(2), Cu1-N3 2.444(2), Cu1-N4 2.470(2), Cu1-N5 1.901(2), N1-Cu1-N2 80.38(9); **2**: Cu1-N1 2.084(2), Cu1-N2 2.048(2), Cu1-N3 2.341(2), Cu1-N4 2.400(2), Cu1-N5 1.869(2), N1-Cu1-N2 82.71(8); **3**: Cu1a-N1a 2.0770(17), Cu1a-N2a 2.1006(17), Cu1a-N3a 2.3687(17), Cu1a-N4a 2.3963(17), Cu1a-N5a 1.8840(18), N1a-Cu1a-N2a 82.13(6).

Complexes **1**-**3** readily crystallize to yield analytically pure solids suitable for single crystal X-ray diffraction studies. Figure 2 shows the solid state structures of these cationic complexes. In all instances the macrocyclic ligand adopts the boat-boat conformation and binds in a κ^4-mode with pyridine units occupying two equatorial positions in the complex with trigonal bipyramidal geometry. We found that the variation of counterion in **1** had little effect of the structure of the

complex. Pyridine ligands in the axial plane feature Cu-N distances within 1.9-2.1 Å – a common value for pentacoordinate Cu(I) species.[49] As expected, amine donors of all macrocycles occupy axial sites of the bipyramid and have slightly longer Cu-N bonds of ca. 2.4 Å.[50] Potentially weaker bonding between the amine donors and the metal in both complexes **1** is manifested in the elongated Cu-N distances in these complexes compared to their less sterically hindered counterparts **2** and **3** (Δ > 0.044 Å).

An intriguing feature of complexes **1**-**3** in the solid state is the tight placement of the pyridine rings within the macrocyclic ligand that may enable the intramolecular interaction between these aromatic units. Interestingly, the pyridine units of these cationic complexes are packed tighter in complexes with greater steric bulk of the substituents at the amine groups of the macrocycle (Figure 2). Namely, the 3.475 or 3.495 Å distance between centroids of pyridine units in complexes **1** is ca. 0.16-0.18 Å shorter than that in the less sterically hindered complex **2** (3.657 Å). This trend is also associated with a drastic change of the angle formed between the pyridine unit planes – the latter is ca. 14% smaller for complexes **1** compared to complex **2**. Taken together, these features suggest that the macrocyclic ligands with high steric hindrance at amine donors allow for shorter intramolecular contacts between pyridine units that can enhance their interaction. Although the characteristic distance between the centroids of two pyridine units in complexes **1**-**3** is longer than that in the free **L1** (Figure 1), only a few known complexes of N,N-dialkyl-2,11-diaza[3.3](2,6)-pyridinophane complexes have been reported to have similar Py-Py distances.[51-53]

Scheme 2. Synthesis of tetragonal halide complexes **4**-**6**
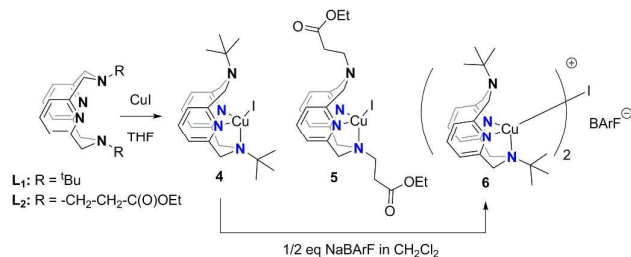
In attempt to further alter the intramolecular contact between aromatic units within Cu complexes we aimed at changing the coordination geometry at the metal center. In copper complexes this can be done by utilizing soft donor ligands that promote the formation of tetrahedral complexes where the pyridinophane ligand would be present in a boat-chair conformation. Indeed, reactions of copper iodide with ligands **L1** and **L2** (Scheme 2) rapidly resulted in the formation of corresponding iodide complexes **4** and **5** that are readily crystallized as yellow-orange, analytically pure solids. Furthermore, inspired by recent remarkable examples of luminescent compounds based on Cu$_2$I$_2$ and Cu$_4$I$_4$ cores[30, 31, 54-56] we attempted the preparation of dinuclear complexes ligated by **L1**. Reaction of complex **4** with 0.5 equivalents of NaBArF as the iodide abstraction agent in dichloromethane

results in rapid precipitation of sodium iodide and formation of complex **6** (Scheme 2).

X-ray structure analysis confirms the tetrahedral coordination geometry in complexes **4**-**6**. The macrocyclic ligand in all complexes adopts a boat-chair conformation and binds in a κ^3-fashion with one amine donor group not bound to copper center. Complexes **4** and **5** have nearly identical Cu1-N3 bond lengths that implies very similar donor ability of the amine ligands of the macrocycles **L1** and **L2**. Consequently, the remote ester group as expected has little effect on the donating strength of the amine group, but rather influences ligand conformation via its reduced steric hindrance. Finally, complex **4** features the shortest distance of 3.349 Å between the centroids of the two pyridine rings among all the complexes studied in this work. The angle between two pyridine rings in **4** is 28.25° that is significantly smaller than the angle in complex **5**, where the pyridine rings are aligned at 43.23°.
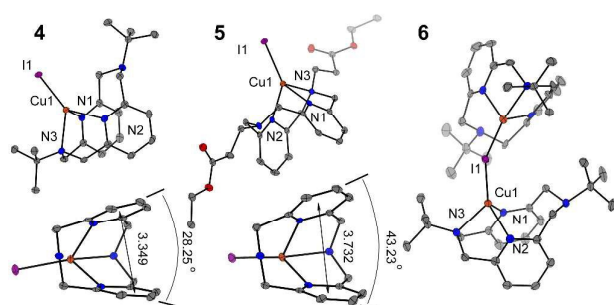
Figure 3. Solid state structures of neutral Cu complexes **4**, **5** and **6**. Thermal ellipsoids are shown on 50% probability level, hydrogen atoms, minor disordered fragments and BArF anion in **6** are omitted for clarity. Ring-ring spacing given for centroids, substituents at amine groups are omitted in the side view projections. Selected bond lengths and angles (Å, °): **4**: Cu1-N1 2.1292(16), Cu1-N2 2.1518(15), Cu1-N3 2.2158(16), Cu1-I1 2.4907(3), N1-Cu1-N2 78.64(6); **5**: Cu1-N1 2.1153(16), Cu1-N2 2.0887(17), Cu1-N3 2.2235(16), Cu1-I1 2.4711(3), N1-Cu1-N2 81.63(6); **6**: Cu1-N1 2.0812(13), Cu1-N2 2.1395(14), Cu1-N3 2.2153(13), Cu1-I1 2.4904(2), N1-Cu1-N2 80.12(5).

Almost exclusively, the shortest contacts between the aromatic groups of **1**-**6** in the solid state are *intramolecular*. For example, the X-ray diffraction data suggests that complexes of **L1** and **L3** have no intermolecular Py-Py contacts in the crystalline state. However, complexes **2** and **5** in solid state demonstrate short intermolecular distances between parallel displaced pyridine units in addition to the intramolecular contacts. The shortest intermolecular Py-Py centroid distances of 3.616 Å (plane shift of 1.572 Å) and 4.740 Å (plane shift of 3.305 Å) were found in **2** and **5**, respectively (see Figure S52 in the Supporting Information). Being similar to the intramolecular Py-Py distance, these structural features may potentially impact the properties of crystalline **2** and **5**.

The comparison of infrared spectra of solid samples complexes **5** and **2** show the presence a C=O stretching band at 1718 cm^{-1} and 1722 cm^{-1}, respectively, typical for carbonyl group of aliphatic esters. IR spectra of cationic complexes **1PF$_6$**, **2**, and **3** exhibit strong band at ~830 cm^{-1}, corresponding to a

non-coordinated PF$_6^-$ counterion. At the same time, complex **1BF$_4$** features strong bands at 1045 cm^{-1} and 1030 cm^{-1} due to the presence of the BF$_4$ counteranion, while the region between 1650 cm^{-1} and 1410 cm^{-1} corresponding to pyridine ring vibrations remains essentially unchanged as compared to **1PF$_6$**. In addition, complex **3** featuring OH groups exhibits free and hydrogen-bound OH stretching vibrations at 3593 cm^{-1} and a broad band at ~3416 cm^{-1}, respectively.
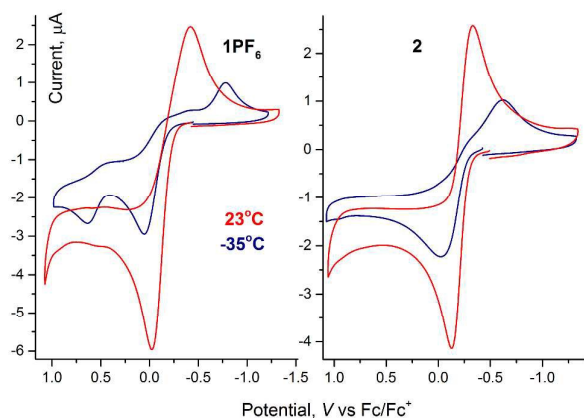
Complexes 1-6 in solution.

Having observed the remarkable difference in structural properties of **1**-**6** in the solid state we further studied how these differences are manifested in solution using NMR spectroscopy. Upon complexation with [Cu(MeCN)$_4$]$^+$ the geminal protons of pyridylmethylenic groups in **L1**-**L3** lose equivalency and appear in ^{1}H NMR spectra at δ 4.65 and 3.43 ppm in CD$_3$CN as two doublets with $^2J_{HH}$ = 15.2 Hz (See Section S2 of the Supporting Information). The macrocyclic ligand in complexes **2** and **3** coordinates exclusively in the κ^4-fashion that is evidenced by the C_{2v} symmetry within the ligand moiety observed by ^{1}H NMR at 23 °C. Unlike **2** and **3**, complexes **1BF$_4$** and **1PF$_6$** feature broad resonances in ^{1}H NMR at 23 °C that resolve at -5 °C. Interestingly, a minor isomer with a κ^3 binding mode could be observed in complexes **1BF$_4$** and **1PF$_6$** in a κ^3/κ^4 = 28.5/71.5 ratio. This conformation is easily distinguished from its κ^4 counterpart owing to the loss of symmetry within the macrocyclic ligand. Namely, the two pyridine backbone protons at *meta* positions appear as separate doublets and pyridylmethylenic protons appear as four doublets with different coupling constants $^2J_{HH}$ of 13 and 15.2 Hz in CD$_3$CN. We attribute this behaviour of **L1**-ligated complexes to the increased steric hindrance imposed by *tert*-butyl substituents that may hinder formation of the κ^4 isomer and lead to the observed exchange.

In agreement with the X-ray diffraction data, the ^{1}H NMR analysis of iodide complexes **4**-**6** confirms their tetrahedral geometry in CD$_2$Cl$_2$ solution (See Supporting Information). This can be deduced from a distinct change of the ligand backbone symmetry in solution when compared to complexes **1**-**3** described above. Namely, the pyridine backbone protons in complex **4** appear as a sharp triplet at δ = 7.25 ppm corresponding to the proton at *para* position while *meta*-H resonances appear as a broad feature at room temperature. At -35 °C it resolves into two doublets at δ = 6.86 and 6.65 ppm with identical $^3J_{HH}$ 7.7 Hz. Methylene groups on the macrocycle appear as four doublets consistent with a C_s symmetric structure. Two separate signals are also observed for N^{t}Bu groups. The ^{1}H NMR spectrum of **6** is nearly identical to that of **4** with the exception of resonances of BArF counterion appearing as singlets at δ = 7.71 and 7.54 ppm.

Interestingly, complexes **4**-**6** are dynamic on the NMR timescale and their resonances are broadened at 23 °C. While the dynamics in **4** and **6** does not involve changes in the coordination mode of the ligand, complex **5** in dichloromethane solution exists as a mixture of a major tetrahedral complex and a minor trigonal bipyramidal complex in a 61/39 ratio at -35 °C. Resonances of complex **5** in ^{1}H NMR coalesce at ca. 10 °C, suggesting a higher exchange rate in

CD$_2$Cl$_2$ in **5** compared to complex **4** with the coalescence temperature of 25 °C (See Figures S27 and S32 in the Supporting Information).


Figure 4. Cyclic voltammograms of solutions of complexes **1PF$_6$** (1 mM) and **2** (1.2 mM) in 0.1M N Bu$_4$ClO$_4$/CH$_3$CN at 23 °C and -35 °C. Scan rate 100 mVs^{-1}; 1.6 mm glassy carbon disk electrode.

Conformational equilibria in acetonitrile solutions of **1** and **2** can also be readily observed with cyclic voltammetry when temperature is varied. At 23 °C, both **1PF$_6$** and **2** show an oxidation wave in MeCN solution with large separation between anodic and corresponding reverse cathodic waves (Figure 4). Similar E$_{1/2}$ = -222.5 mV and -229.5 mV vs. Fc/Fc$^+$ measured at 23 °C for complexes **1PF$_6$** (Figure 4, left, red line) and **2** (Figure 4, right, red line) respectively, implies that the electronic properties of the remote ester functional group do not significantly affect the electronics at the metal center. In line with NMR data that suggests the existence of two conformations in **1PF$_6$**, at -35 °C this complex features two oxidation waves, at 59 and 640 mV vs Fc/Fc$^+$, assigned to the species with κ^4- and κ^3-bound ligands respectively (Figure 4).[50] By contrast, complex **2**, shown to exist as a single conformer in solution by ^{1}H NMR, correspondingly revealed a single oxidation event even at -35 °C (Figure 4).

Photophysical studies.

Complexes **1**-**6** absorb light in near UV region in the solid state. Microspectrophotometry analysis of crystalline samples revealed the broad absorption bands in the 300-500 nm range with peak maxima of ca. 395-420 nm (see Figure S37 in the Supporting Information). When dissolved in CH$_3$CN or CH$_2$Cl$_2$, complexes **1**-**6** feature similar intense absorption bands in the deep UV region at 250-300 nm associated with ligand π-π* transitions and less intense broad metal-to-ligand charge-transfer bands at 395-400 nm (see Figure 5 and Figure S38 in the Supporting Information). The free ligands **L1**-**L3** shows similar π-π* transitions at 260-270 nm, having negligible absorption above 300 nm (see Figure S37 in Supporting Information).
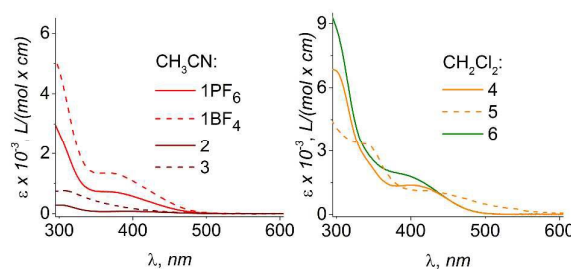

Figure 5. UV-Vis absorbance spectra for complexes **1-6** in dichloromethane and acetonitrile solutions in 300-600 nm region.

Upon irradiation with 400 nm light, complexes **1-6** emit visible light in the solid state. Emission colour varied from red to green depending on the complex used. While cationic complexes **1**-**3** emit red light at 619 (identical for **1PF$_6$** and **1BF$_4$**), 637 (**2**) and 665 (**3**) nm, the neutral iodide complexes emit light at 585 (**4**), 564 (**5**) and 524 (**6**) nm (Figure 6 A). The photoluminescence lifetimes determined by time-resolved photoluminescence measurements were in range of 2-30 µs (see Table 1).

Interestingly, complex **5** had a distinctly different photoluminescence decay profile in the crystalline state (See Figure S41 in the Supporting Information). Unlike its counterparts, complex **5** was found to have two decay components in the crystalline state with lifetimes of τ = 0.97 and 6.59 µs. Such behaviour in crystalline **5** can occur due to intermolecular interactions, i.e. formation of excimers, that was consistent with our X-ray diffraction studies showing relatively short intermolecular Py-Py distances (Figure S52 in the Supporting Information) (vide supra). We found that the emission of the long lived component was significantly red-shifted compared to the short lived component (Figure S44 in the Supporting information). To assign the decay components to particular state of complex **5** we analysed the emission of amorphous **5** blended into a PMMA film where the formation of excimers would be less favourable. We found that amorphous **5** emits at λ$_{max}$ = 610 nm that is ca. 45 nm red-shifted from the crystalline **5**. We, therefore, conclude that a long lived red-shifted component is produced by monomeric **5** rather than its excimers. Interestingly, complex **2** – the cationic counterpart of **5**, features a simple monoexponential decay suggesting that the presence of intermolecular aggregation does not necessarily contribute to emission.

ARTICLE

Journal Name
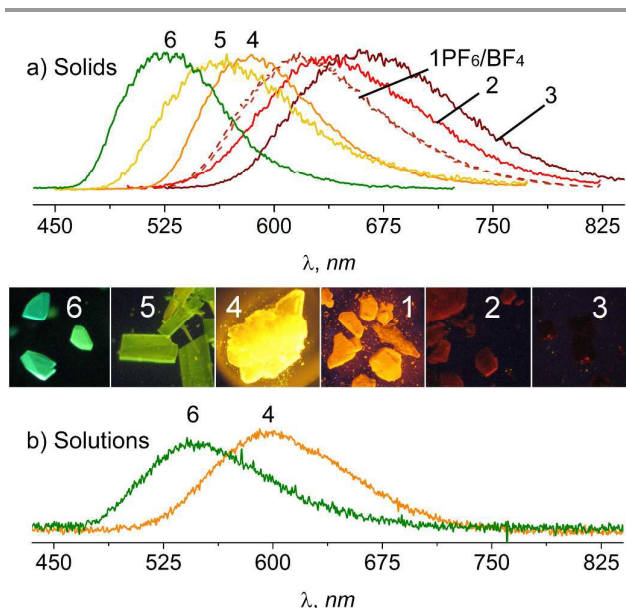
Figure 6. Normalized emission spectra of complexes **1**-**6** in solid state (a) and in CH_2Cl_2 solution (b) at T = 23 °C; excitation at 400 nm. Photographs of crystalline samples are taken with 365 nm light excitation.

The absolute luminescence quantum yield of copper complexes varied significantly from 0.02 to 0.78. Interestingly, the quantum yield and the spatial arrangement of the pyridine rings within the ligand were correlated: complexes with tight intramolecular distances between two pyridine rings were more efficient emitters. Namely, cationic pentacoordinate complexes **1BF₄** and **1PF₆** that have tight pyridine-pyridine distances have a quantum yield that is at least 10-fold higher than analogous complexes **2** and **3**. The same trend is observed in iodide complexes **4**, **6** and **5** where the latter has the longest pyridine-pyridine centroid distance and the lowest corresponding quantum yield.

Much to our satisfaction, the impact of intramolecular interactions in complexes **4** and **6** is sufficient to enable

Table 1. Summary of absorption and emission characteristics of complexes **1**-**6** in the crystalline state

Complex	λ_{emi}, nm	CIE color coordinates (x,y)[g]	Φ^{a}	τ, µs	k_{rad}, $10^{-3}s^{-1}$	d_{Py-Py}, Å [b]
1PF₆	619	0.5938,0.4043	0.35	30.05	11.64	3.4950(16)
1BF₄	619	0.5889,0.4093	0.30	24.79	12.10	3.4752(12)
2	637	0.6036,0.3940	0.03	18.20	1.77	3.6568(13)
3	665	0.6486,0.3507	0.02	2.63	9.46	3.6211(12) and 3.5806(12)[e]
4	585	0.5142,0.4756	0.78	15.79	49.40	3.3494(10)
5	564	0.4388,0.5375	0.08	2.31[c]	34.63[d]	3.7315(12)
6	524	0.2798,0.5906	0.53	13.90	38.13	3.4647(11) and 3.595(7)/ 3.611(8)[f]

[a] absolute quantum yield, all measurements performed with excitation at 400 nm; [b] solid state distance between centroids built on pyridine units; [c] weighed average value derived from the two component fitting, see section S2 in the Supporting Information for decay profiles; [d] calculated using weight averaged lifetime value; [e] values for the symmetrically independent molecules A and B, respectively; [f] values for the first unit and both disordered components of the second unit of binuclear complex **6**, respectively; [g] CIE 1931, chromaticity diagram containing solid and solution state data can be found on Figure S46 of the supporting information .

photoluminescence even in solution. Complex **4** emits yellow-orange light (CIE (0.527,0.4512)) at 600 nm in dichloromethane with absolute quantum yield of 0.28 (Figure 6 B). Its halide-bridged counterpart **6** emits green light (CIE (0.3719,0.5375)) at 545 nm with a quantum yield of 0.15. Interestingly, the emission integral intensity and absorbance of **4** and **6** is directly proportional to their concentration (See Figure S43 Supporting Information) confirming their nature as molecular emitters that are unaffected by intermolecular forces. Furthermore, the solution-like emission characteristics were observed for PMMA films containing complexes **4** and **6**.Very marginally affected by a change of the aggregation state, films containing **4** emit at 580 nm with a quantum yield of 0.29 and films fabricated with complex **6** emit with Φ = 0.26 at 548 nm (See Figure S45 in the Supporting Information).

The emission lifetime of complexes **4** and **6** in dichloromethane is considerably lower than that in the solid state. Time resolved photoluminescence spectroscopy measurements estimate the lifetimes to be 4.3 µs for complex **4** and 0.9 µs for complex **6** in CH_2Cl_2. We attribute the lifetime

decrease to the prevalence nonradiative relaxation pathways expected to take effect in solution. Namely, chemical exchange associated with the solution dynamics of the pyridinophane macrocycle may be one of the major contributors to the nonradiative relaxation.

On the origin of the emission.

Our structural and photophysical data suggests that intramolecular Py-Py interactions have a crucial effect on the emissive properties of pyridinophane complexes. In this respect, it is particularly important to reveal the electronic transitions involved in photoluminescence. Having complex **4** as the representative example we analyzed its electronic structure using DFT calculations to identify the photophysical events leading to emission.

Frontier orbital analysis shows that the HOMO orbital in **4** in the ground state is confined mainly to Cu and I centers (57 % and 23 %, Figure 7 A) with lower energy HOMO-1 orbital having similar character. The spatially separated pyridine rings are directly involved in the formation of the excited S_1 state of

complex **4** since they form the LUMO orbital set that is confined to both pyridine rings (44 % and 48 % for Py units in LUMO, Figure 6 A). Interestingly, parts of LUMO confined to different Py rings have a positive overlap, therefore, population of LUMO should enhance the interaction between the Py units.
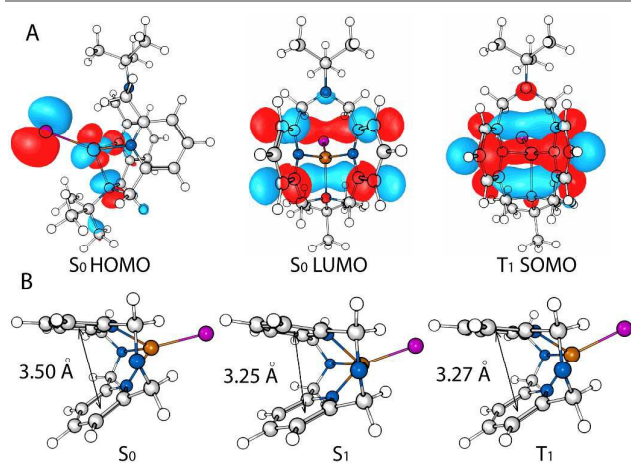
Figure 7. DFT computed (A) frontier HOMO/LUMO orbitals of complex **4** in the ground state S_0 and the highest populated SOMO orbital of T_1 state in CH_2Cl_2 at isosurface value 0.03 and (B) optimized structures of S_0, S_1 and T_1 states. ^{t}Bu substituents omitted for clarity, the values indicated correspond to the distances between centroids built on pyridine units.

TD-DFT analysis predicts the S_0-S_1 transition to have mixed metal-to-ligand and halide-to-ligand charge-transfer (M+X)LCT character associated with calculated absorption at 385 nm. In agreement with theoretical prediction the lowest energy absorption band was experimentally observed at 400 nm, a common value for MLCT/XLCT bands in Cu complexes.[17] The nature and localization of the LUMO orbitals that are populated upon excitation is the major factor governing the emission. When the LUMO orbital set is populated during excitation one would expect the strong attractive forces to emerge that, in turn, should alter the geometry of the excited state. Indeed, the TD-DFT analysis indicates the contraction of the Py-Py spacing by $\Delta = 0.25$ Å upon the formation of the first excited state S_1 (Figure 6 B).

As the emission lifetimes observed for complex **4** are relatively long (15.79 µs in the solid state and 4.3 µs in solution), the possible contribution of the triplet state to overall emission is likely. In agreement with this suggestion, DFT analysis estimates the emission maxima for the triplet state at 614 nm while the S_1 state would emit at 557 nm. Interestingly, the relaxation of the T_1 state geometry that precedes the emission is also associated with the rearrangement of the stacking pyridine units within **4**. Similar to S_1, the T_1 state has a significantly shorter Py-Py contacts compared to the ground state ($\Delta = 0.23$ Å). As expected, formation of T_1 state strengthens the interaction between the Py units in macrocyclic ligand as evidenced by the frontier orbital analysis. Namely, the population of LUMO level in S_0 results in formation of the new SOMO of T_1 featuring a positive

overlap between the Py units (Figure 6 A). Similar to the LUMO of S_0, the higher energy SOMO of T_1 is almost exclusively confined to pyridine units (52 and 41 % for each Py unit). This, in turn, suggests stronger bonding between the Py units in T_1 compared to the ground state.

In summary, pyridine units in complex **4** not only interact but directly influence its emissive properties in two ways. Firstly, they provide electron accepting LUMO orbitals in the ground state (S_0) confined exclusively to the pyridine units. Secondly, the interaction between pyridine units strengthens upon excitation and directs the formation of stable geometries of excited S_1 and T_1 states – the crucial step that precedes emission.

Conclusion

In conclusion, we have developed a new class of transition metal-based compounds that rely on intramolecular non-covalent interactions to enable photoluminescence. In contrast to the majority of emissive TM complexes that are tuned via modification of the donor/acceptor properties of their ligand, the compounds reported in this work are tuned by the variation of *steric* properties of macrocyclic ligands that impacts the intramolecular non-covalent interactions within the ligand molecule.

As a result, simple pyridinophane macrocycles act as potent and tunable ligands that yield copper(I) complexes emitting in the range of 524-665 nm with a quantum yield up to 78% at 23 °C. Due to the molecular nature of emission, complexes **4** and **6** are capable of solution state emission with quantum yields of 28 and 15 % correspondingly. Our experimental data suggests a strong link between the extent of intramolecular aromatic interaction and the quantum yield of photoluminescence and DFT calculations explain how these interactions are involved in the formation of emissive states. Finally, our results introduce a new strategy for designing photoluminescent compounds that employs subtle conformational modifications as the main tuning motif. Being intrinsically sensitive to the local steric environment, the new emissive complexes hold a good potential to be utilized in sensing and imaging applications.
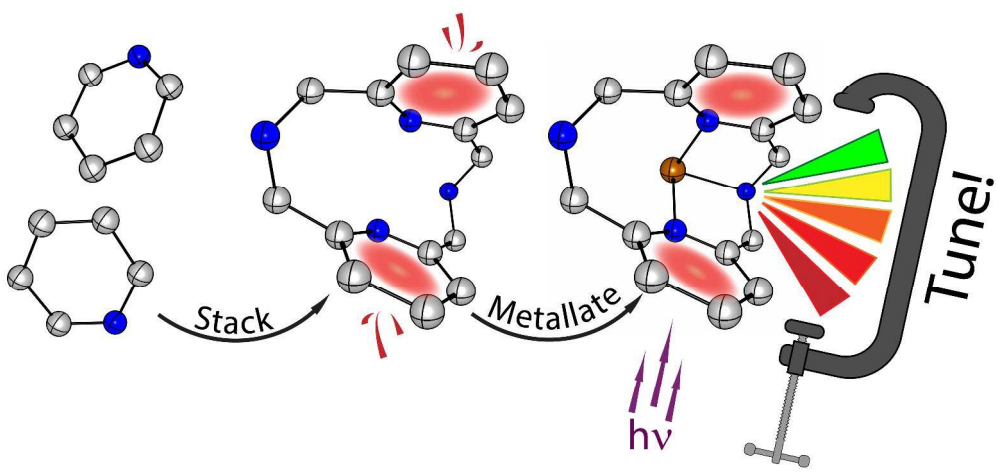
Acknowledgements

Notes and references

1   R. C. Evans, P. Douglas and C. J. Winscom, *Coord. Chem. Rev.*, 2006, **250**, 2093-2126.

ARTICLE

Journal Name

2   J. Wu, W. Liu, J. Ge, H. Zhang and P. Wang, *Chem. Soc. Rev.*, 2011, **40**, 3483-3495.

3   K. Li, W. Qin, D. Ding, N. Tomczak, J. Geng, R. Liu, J. Liu, X. Zhang, H. Liu, B. Liu and B. Z. Tang, *Sci. Rep.*, 2013, **3**, 1150.

4   Z. Wang, J. Nie, W. Qin, Q. Hu and B. Z. Tang, *Nat. Commun.*, 2016, **7**.

5   S. Lee, S.-O. Kim, H. Shin, H.-J. Yun, K. Yang, S.-K. Kwon, J.-J. Kim and Y.-H. Kim, *J. Am. Chem. Soc.*, 2013, **135**, 14321-14328.

6   F. Julia, D. Bautista, J. M. Fernandez-Hernandez and P. Gonzalez-Herrero, *Chem. Sci.*, 2014, **5**, 1875-1880.

7   X. Yan, T. R. Cook, P. Wang, F. Huang and P. J. Stang, *Nat. Chem.*, 2015, **7**, 342-348.

8   R. Sakamoto, T. Iwashima, J. F. Kögel, S. Kusaka, M. Tsuchiya, Y. Kitagawa and H. Nishihara, *J. Am. Chem. Soc.*, 2016, **138**, 5666-5677.

9   T. Seki, Y. Takamatsu and H. Ito, *J. Am. Chem. Soc.*, 2016, **138**, 6252-6260.

10 D. Volz, M. Wallesch, C. Flechon, M. Danz, A. Verma, J. M. Navarro, D. M. Zink, S. Brase and T. Baumann, *Green Chem.*, 2015, **17**, 1988-2011.

11 N. Armaroli, G. Accorsi, F. o. Cardinali and A. Listorti, in *Photochemistry and Photophysics of Coordination Compounds I*, Springer Berlin Heidelberg, Berlin, Heidelberg, 2007, 280, 69-115.

12 P. C. Ford, E. Cariati and J. Bourassa, *Chem. Rev.*, 1999, **99**, 3625-3648.

13 A. l. Lavie-Cambot, M. Cantuel, Y. Leydet, G. Jonusauskas, D. M. Bassani and N. D. McClenaghan, *Coord. Chem. Rev.*, 2008, **252**, 2572-2584.

14 O. Horváth, *Coord. Chem. Rev.*, 1994, **135**, 303-324.

15 T. Hofbeck, U. Monkowius and H. Yersin, *J. Am. Chem. Soc.*, 2015, **137**, 399-404.

16 S. B. Harkins and J. C. Peters, *J. Am. Chem. Soc.*, 2005, **127**, 2030-2031.

17 A. Tsuboyama, K. Kuge, M. Furugori, S. Okada, M. Hoshino and K. Ueno, *Inorg. Chem.*, 2007, **46**, 1992-2001.

18 M. Nishikawa, Y. Wakita, T. Nishi, T. Miura and T. Tsubomura, *Dalton. Trans.*, 2015, **44**, 9170-9181.

19 D. R. McMillin and K. M. McNett, *Chem. Rev.*, 1998, **98**, 1201-1220.

20 G. Blasse and D. R. McMillin, *Chem. Phys. Lett.*, 1980, **70**, 1-3.

21 D. G. Cuttell, S.-M. Kuang, P. E. Fanwick, D. R. McMillin and R. A. Walton, *J. Am. Chem. Soc.*, 2002, **124**, 6-7.

22 C. Bizzarri, C. Strabler, J. Prock, B. Trettenbrein, M. Ruggenthaler, C.-H. Yang, F. Polo, A. Iordache, P. Braggeller and L. D. Cola, *Inorg. Chem.*, 2014, **53**, 10944-10951.

23 M. Nishikawa, T. Sano, M. Washimi, K. Takao and T. Tsubomura, *Dalton. Trans.*, 2016, **45**, 12127-12136.

24 V. A. Krylova, P. I. Djurovich, M. T. Whited and M. E. Thompson, *Chem. Commun.*, 2010, **46**, 6696-6698.

25 V. A. Krylova, P. I. Djurovich, J. W. Aronson, R. Haiges, M. T. Whited and M. E. Thompson, *Organometallics*, 2012, **31**, 7983-7993.

26 V. A. Krylova, P. I. Djurovich, B. L. Conley, R. Haiges, M. T. Whited, T. J. Williams and M. E. Thompson, *Chem. Commun.*, 2014, **50**, 7176-7179.

27 R. Marion, F. Sguerra, F. Di Meo, E. Sauvageot, J.-F. o. Lohier, R. Daniellou, J.-L. Renaud, M. Linares, M. Hamel and S. Gaillard, *Inorg. Chem.*, 2014, **53**, 9181-9191.

28 A. J. M. Miller, J. L. Dempsey and J. C. Peters, *Inorg. Chem.*, 2007, **46**, 7244-7246.

29 K. J. Lotito and J. C. Peters, *Chem. Commun.*, 2010, **46**, 3690-3692.

30 Y. Okano, H. Ohara, A. Kobayashi, M. Yoshida and M. Kato, *Inorg. Chem.*, 2016, **55**, 5227-5236.

31 H. Araki, K. Tsuge, Y. Sasaki, S. Ishizaka and N. Kitamura, *Inorg. Chem.*, 2005, **44**, 9667-9675.

32 C. T. Cunningham, K. L. H. Cunningham, J. F. Michalec and D. R. McMillin, *Inorg. Chem.*, 1999, **38**, 4388-4392.

33 C.-M. Che, Z.-Y. Li, K.-Y. Wong, C.-K. Poon, T. C. W. Mak and S.-M. Peng, *Polyhedron*, 1994, **13**, 771-776.

34 J. Mei, N. L. C. Leung, R. T. K. Kwok, J. W. Y. Lam and B. Z. Tang, *Chem. Rev.*, 2015, **115**, 11718-11940.

35 Y. Hong, J. W. Y. Lam and B. Z. Tang, *Chem. Commun.*, 2009, 4332-4353.

36 X. Zhang, Z. Chi, Y. Zhang, S. Liu and J. Xu, *J. Mater. Chem. C*, 2013, **1**, 3376-3390.

37 T. U. Connell, J. M. White, T. A. Smith and P. S. Donnelly, *Inorg. Chem.*, 2016, **55**, 2776-2790.

38 Q. Zhao, L. Li, F. Li, M. Yu, Z. Liu, T. Yi and C. Huang, *Chem. Commun.*, 2008, 685-687.

39 G.-G. Shan, H.-B. Li, H.-Z. Sun, D.-X. Zhu, H.-T. Cao and Z.-M. Su, *J. Mater. Chem. C*, 2013, **1**, 1440-1449.

40 K. Huang, H. Wu, M. Shi, F. Li, T. Yi and C. Huang, *Chem. Commun.*, 2009, 1243-1245.

41 Y. You, H. S. Huh, K. S. Kim, S. W. Lee, D. Kim and S. Y. Park, *Chem. Commun.*, 2008, 3998-4000.

42 M. Osawa, *Chem. Commun.*, 2014, **50**, 1801-1803.

43 R.-H. Wei, J.-F. Chen, J.-Q. Feng, J.-S. Hu and D.-K. Cao, *RSC Adv.*, 2015, **5**, 14359-14365.

44 J. R. Khusnutdinova, N. P. Rath and L. M. Mirica, *Inorg. Chem.*, 2014, **53**, 13112-13129.

45 S. P. Meneghetti, P. J. Lutz and J. Kress, *Organometallics*, 2001, **20**, 5050-5055.

46 F. Bottino, M. Di Grazia, P. Finocchiaro, F. R. Fronczek, A. Mamo and S. Pappalardo, *J. Org. Chem.*, 1988, **53**, 3521-3529.

47 N. A. Yakelis and R. G. Bergman, *Organometallics*, 2005, **24**, 3579-3581.

48 G. J. Kubas, B. Monzyk and A. L. Crumblis, in *Inorganic Syntheses*, John Wiley & Sons, Inc., 2007, 68-70.

49 S. Holler, M. Tüchler, F. Belaj, L. F. Veiros, K. Kirchner and N. C. Mösch-Zanetti, *Inorg. Chem.*, 2016, **55**, 4980-4991.

50 J. R. Khusnutdinova, J. Luo, N. P. Rath and L. M. Mirica, *Inorg. Chem.*, 2013, **52**, 3920-3932.

51 W.-T. Lee, S. B. Muñoz, D. A. Dickie and J. M. Smith, *Angew. Chem. Int. Ed.*, 2014, **53**, 9856-9859.

52 W. O. Koch and J. T. Kaiser, *Chem. Commun.*, 1997, 2237-2238.

53 M. Jagoda, S. Warzeska, H. Pritzkow, H. Wadepohl, P. Imhof, J. C. Smith and R. Krämer, *J. Am. Chem. Soc.*, 2005, **127**, 15061-15070.

54 K. Tsuge, *Chem. Lett.*, 2013, **42**, 204-208.

55 S. Perruchas, X. F. Le Goff, S. Maron, I. Maurin, F. Guillen, A. Garcia, T. Gacoin and J.-P. Boilot, *J. Am. Chem. Soc.*, 2010, **132**, 10967-10969.

56 M. Vitale and P. C. Ford, *Coord. Chem. Rev.*, 2001, **219-221**, 3-16.

2081x1040mm (72 x 72 DPI)